ACS APPLIED MATERIALS & INTERFACES

www.acsami.org Research Article

Directional Copper Decoration of Spaced TiO_2 Nanotubes Enables Geometry-Controlled Ion Release and Antibacterial Response

Markus Pach, David Böhringer, Iana Fomicheva, George Sarau, Nicola Taccardi, Maksim Kamaleev, Silke H. Christiansen, Wolfgang H. Goldmann, Alexander B. Tesler,* and Anca Mazare*

Cite This: *ACS Appl. Mater. Interfaces* 2026, 18, 6157−6165 Read Online

ACCESS | Metrics & More | Article Recommendations | Supporting Information

ABSTRACT: Anodic titanium dioxide (TiO_2) nanotubes (NTs) are well-established implant coatings owing to their nanoscale tunability, osteogenic support, and long-term biocompatibility. However, reproducible approaches that directly link NT geometry with controlled antibacterial functionality and tunable ion release remain limited. Here, we present a spatially selective, geometry-defined copper (Cu) decoration strategy for morphology-defined spaced NTs with an intertube spacing of 70−214 nm and a diameter of ∼145 nm. These NTs were fabricated via fluoride-containing diethylene glycol-based anodization. Directional sputtering was used to deposit Cu as either conformal wall coatings, the common physical vapor deposition configuration, or as discrete top caps, perpendicular to the sputtering target configuration, thus enabling precise control of the Cu metal localization on/in the spaced NTs. Morphology−composition correlations, confirmed by scanning electron microscopy (SEM), energy-dispersive X-ray spectroscopy (EDX), X-ray photoelectron spectroscopy (XPS), and focused ion beam scanning electron microscopy (FIB-SEM), revealed a clear depth confinement for the cap-decorated NTs versus an extended distribution in the case of the conformal coatings. Inductively coupled plasma atomic emission spectroscopy (ICP-AES) showed that ∼1 atom % Cu, the antibacterial/cytocompatibility threshold in the literature, generated sustained ion release with early bacterial suppression. Higher loadings accelerated Cu^{2+} release but produced variable long-term inhibition, which can be correlated with the Cu configuration type. This geometry-directed sputtering approach provides a reproducible route for spatially controlled Cu placement, with a link between NT geometry, Cu localization, and antibacterial behavior, thus applicable for designing future multifunctional implant surfaces with controlled therapeutic release. It also provides a reproducible strategy for designing future multifunctional, release-tunable implant surfaces.

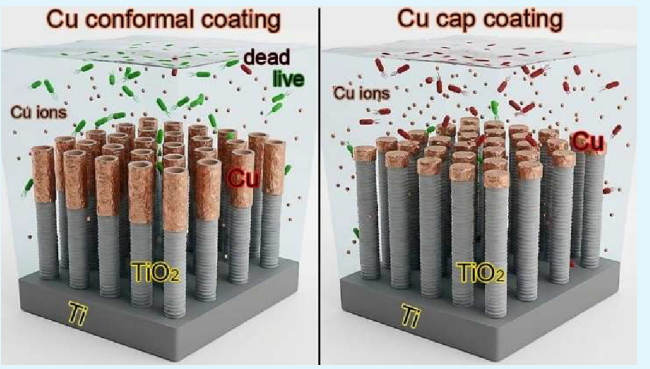

KEYWORDS: *spaced TiO_2 nanotubes, copper decoration, controlled ion release, antibacterial implant surfaces, electrochemical anodization*

Downloaded via FRIEDRICH-ALEXANDER-UNIV on January 31, 2026 at 14:43:33 (UTC).
See https://pubs.acs.org/sharingguidelines for options on how to legitimately share published articles.

1. INTRODUCTION

Titanium (Ti) and its alloys are widely used in orthopedic and dental implants due to their mechanical durability, corrosion resistance, and long-term biocompatibility. To further improve tissue integration, anodically formed titanium dioxide (TiO_2) nanotubes (NTs) have emerged as a leading surface engineering strategy. They provide vertically aligned arrays with a high surface area, controllable nanoscale dimensions, and reproducible fabrication.[1−3] Such architectures enhance osseointegration and direct cell guidance, and they also serve as versatile platforms for therapeutic functionalization. This enables the incorporation of bioactive agents directly within the nanotube structure.[3−5]

Among nanotopographical design parameters, the spacing between TiO_2 nanotubes (NTs) has emerged as a critical factor influencing cellular behavior and subsequent functionalization.[6,7] Spaced NTs, defined by controlled separations between neighboring tubes, facilitate direct access for nanoparticle deposition or ion loading and mitigate the clogging effects often observed in close-packed architectures.[8,9] In biomedical contexts, nanoscale spacing influences focal adhesion formation and integrin clustering, both central to osteogenic differentiation.[3−5] Thus, spacing is a structural parameter of equal importance to tube diameter. Despite their proven advantages for biointegration and surface modification, spaced NTs have been scarcely investigated as scaffolds for antibacterial surface design.

Received: October 15, 2025
Revised: January 5, 2026
Accepted: January 5, 2026
Published: January 15, 2026

ACS Publications © 2026 American Chemical Society

Nanostructured implant surfaces can modulate bacterial adhesion through a combination of physical and biochemical mechanisms.[10,11] At the submicron scale, the interfeature spacing dictates how bacteria position themselves, whether by bridging gaps or adhering to individual nanostructures. This, in turn, influences membrane tension and mechanosensitive signaling. Spacings of ∼100−200 nm have been shown to induce localized mechanical stress and stimulate exopolysaccharide (EPS) production. In some cases, these spacings can lead to membrane rupture, particularly in Gram-negative bacteria.[10] Additional factors, such as surface wettability and geometry-driven rinsing, also influence bacterial retention.[11] Thus, spaced TiO_2 NTs offer structural advantages and provide an open architecture that is ideally suited for incorporating antibacterial agents, such as metal ions, for localized therapeutic release.

Postsurgical infection is a critical complication in implantology that frequently results in chronic inflammation, compromised osseointegration, and eventual implant failure. Although silver (Ag) coatings are widely used due to their potent, broad-spectrum antibacterial activity, their clinical use is limited by high cytotoxicity at elevated release levels, poor long-term ion stability, and increasing reports of bacterial resistance.[12,13]

The functionalization of TiO_2 nanostructures with copper (Cu) is a promising alternative that offers strong antibacterial activity and lower cytotoxicity risks when optimally dosed. Reported strategies for Cu incorporation include electrochemical (e.g., electrodeposition), chemical (e.g., solution-based, photochemical, etc.), and physical vapor deposition (PVD) on anodic TiO_2 NTs of different morphology (e.g., close-packed anodic NTs,[14−18] or spaced NTs[19]) or Cu−Ti−O nanotubes from TiCu sputtered layers.[20] TiCu cosputtering can be applied to both thicker and thinner layers.[20,21] Hydrothermally grown NTs,[22] nanorods modified by ion implantation,[23] and porous TiO_2 layers formed via microarc oxidation (MAO), with Cu introduced either during[24,25] or after[26] the MAO process.

Typical copper (Cu) decoration techniques, particularly electrochemical and chemical deposition routes on close-packed nanotubes (NTs), often result in uncontrolled Cu nucleation. This usually produces bottom-initiated filling, large agglomerates, or patchy particle distributions.[14−18] This occurs because deposition is dictated by local conductivity, surface defects, or solution chemistry rather than geometric selectivity. Consequently, Cu often accumulates inside the tubes and clogs the interior of nanotubes, preventing spatial confinement to specific regions. Overall, these decoration methods offer limited control over the spatial distribution of Cu within the nanostructure. Few, if any, establish quantitative links between Cu localization, release kinetics, and antibacterial performance.

Usually, sputtering approaches employed to decorate TiO_2 NTs lead to either a minimal decoration at the tube mouth or top[27] (which depends on the sputtered material and follow-up annealing treatment, as under some specific conditions the sputtered material can coalesce and/or dewet to a nanoparticulate form),[28] or to a conformal tube wall decoration to a certain degree.[29] Only recently, sputtering was used as a conformal coating with higher Au loading for plasmonic application on spaced NTs.[30] In contrast to close-packed NTs, the open architecture of spaced NTs reduces shadowing by increasing the lateral spacing between nanotubes. Combined with directional sputtering, this enables true, geometry-defined copper (Cu) location. This allows for either discrete caps at the tube openings or controlled, conformal wall coatings.

In this study, we present a directional sputtering strategy that enables geometry-defined Cu decoration of spaced TiO_2 NTs. This decoration can be achieved as either a conformal wall coating or discrete top caps at the tube openings. This spatial selectivity allows for the precise modulation of Cu content, localization, and dissolution behavior in a single-step process. Unlike prior electrodeposition- or MAO-based approaches on close-packed NTs or porous TiO_2,[14,15,19,22] our method achieves controlled Cu placement without aggregation, while preserving the nanotubular architecture. By correlating deposition geometry with Cu^{2+} ion release kinetics and antibacterial response, we demonstrate a geometry-dependent relationship between NT morphology and surface performance. This reproducible approach can be a foundation for future engineering of multifunctional implant coatings with tunable antibacterial activity and long-term structural stability.

2. RESULTS AND DISCUSSION

Scheme 1 illustrates the process of forming the directional Cu layer decoration of spaced TiO_2 nanotubes. Anodic TiO_2

Scheme 1. Schematic Illustrating the Process of Directionally Decorating Spaced TiO_2 Nanotubes with Copper (Cu)[a]

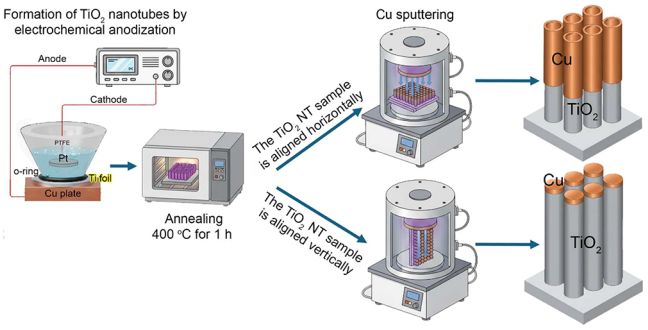

[a]First, anodic compact or spaced TiO_2 nanotubes are formed through electrochemical anodization. Then, they are annealed to form an anatase crystalline structure. Second, directional Cu decoration was achieved by aligning the sample vertically or horizontally to the sputtering target, whether on the top or for a conformal wall coating.

nanotube layers with varied morphologies and a fixed outer diameter of ∼145 nm were fabricated through electrochemical anodization. For spaced NTs, the intertube spacing (S) was tuned across three distinct regimes: $S \approx 70$, $S \approx 135$, and $S \approx 210$ nm (Figure 1a). These morphologies were obtained by adjusting the water content in diethylene glycol (DEG)-based hydrofluoric acid (HF) electrolytes, resulting in systematically controlled spaced (SP) NTs (see the Section 4). For reference, a close-packed (CP) NT layer was produced by anodizing in a conventional fluoride-containing, organic-based electrolyte (70% glycerol and 30% water). High-resolution scanning electron microscopy (SEM) imaging confirmed the formation of vertically aligned, open-top TiO_2 nanotubes with homogeneous coverage across the substrates (Figures 1a and S1). Subsequent annealing at 400 °C in air for 1 h converted the amorphous layers to anatase (Scheme 1).

Figure 1b shows a quantitative comparison of SP NT morphologies, including tube diameter, intertube spacing, and

https://doi.org/10.1021/acsami.5c20633
ACS Appl. Mater. Interfaces 2026, 18, 6157−6165

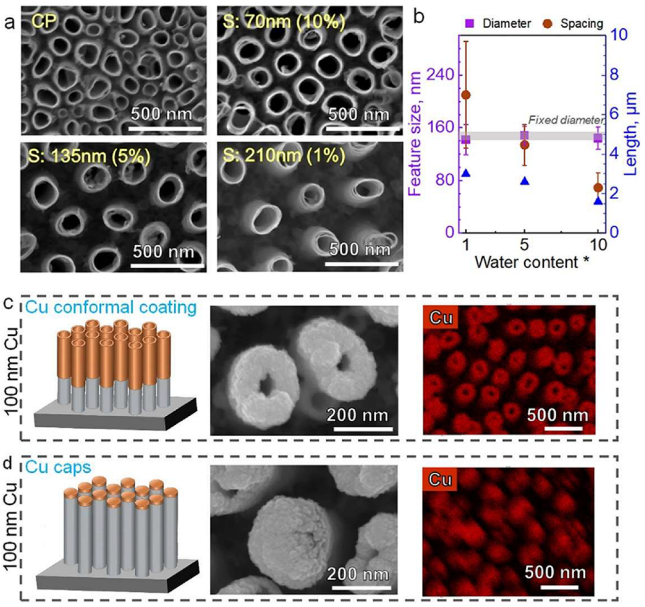

Figure 1. (a) High-resolution scanning electron microscopy (SEM) images showing the top morphologies of close-packed (CP) and spaced (SP) nanotubes, with spacings ranging from 70 to 210 nm for the latter; (b) overview of the feature sizes (diameter and spacing) and lengths for the spaced nanotubes; (c) and (d) Cu conformal coatings and Cu caps, with a schematic and SEM images showing the nominal of 100 nm thick sputtered Cu and SEM-EDX Cu maps.

tube length as a function of electrolyte water content. These values were obtained through a statistical evaluation of multiple scanning electron microscopy (SEM) measurements across each sample. Although all anodization experiments were carried out for 20 h, the applied potential was adjusted for each condition (i.e., electrolyte composition) to maintain a comparable tube diameter of ~145 nm. As an overview, ~70 nm spaced NTs have a tube diameter of ~144 ± 17 nm and spacing of ~69 ± 23 nm, ~135 nm spaced NTs have diameters of ~148 ± 14 nm and spacings of ~134 ± 31 nm, and ~215 nm spaced NTs have diameters of ~142 ± 23 nm and spacings of ~213 ± 79 nm. As intertube spacing increased, tube length increased moderately, likely due to different growth rates resulting from differences in electrolyte composition and conductivity (due to the lower water content) (Figure S1).[31] Histograms for the tube diameter and spacing for the selected morphology with 135 nm spacing for spaced NTs are shown in Figure S2. The as-prepared CP and spaced NTs are superhydrophilic, as detailed in Supporting Information and the shown water contact angles of Figure S3.

More importantly, the decoupling of spacing from tube diameter isolates the effect of lateral geometry, enabling a direct comparison of how identical-diameter and comparable length NTs with varied spacing influence Cu deposition depth and subsequent release kinetics. This is particularly relevant because in earlier Cu-decorated TiO_2 systems, tube geometry and functionalization were often codependent.[14,15,19,22]

To evaluate the influence of deposition geometry on Cu distribution within the NTs, Cu was sputtered onto spaced NTs with 135 nm intertube spacing under two distinct orientations at a nominal thickness of 100 nm. When the substrate was aligned parallel to the target (Scheme 1, top route), a conformal coating was obtained with Cu distributed uniformly along the tube walls (Figures 1c and S4a). In contrast, perpendicular sputtering, i.e., the sample aligned perpendicular to the substrate (Scheme 1, bottom route), produced discrete Cu caps localized at the tube openings, reflecting the line-of-sight nature of the deposition process (see Figures 1d and S4b).

In the conformal case, the metallic Cu layer extended from the top of the NT into the tube's depth (Figures 1c and S4a). In contrast, the cap morphology produced sharp, well-defined features confined to the tube's surface (Figures 1d and S4b). SEM and energy-dispersive X-ray (EDX) mapping corroborate this distinction (Figures 1c,d and S5–S7). These analyses confirmed the spatial confinement of Cu in the cap configuration and demonstrated the directional selectivity of the sputtering process. For the CP NT architecture, however, the contrast between the two morphologies was markedly reduced (Figure S5). This is likely due to the limited intertube spacing, which restricts directional flux penetration and promotes the lateral scattering of sputtered species.

Adjusting the sputtering angle is a consistent and straightforward way to control the depth and location of Cu within the NT geometry, allowing for selective functionalization. This control over the loading architecture directly affects the surface's antibacterial performance. To visualize the distribution, focused ion beam (FIB) cross sections with corresponding scanning electron microscopy (SEM)-energy dispersive X-ray spectroscopy (EDX), elemental maps were obtained for 100 nm Cu (nominal mass thickness as obtained by the quartz crystal microbalance) deposition in both configurations on the 135 nm spaced TiO_2 NTs (Figure 2).

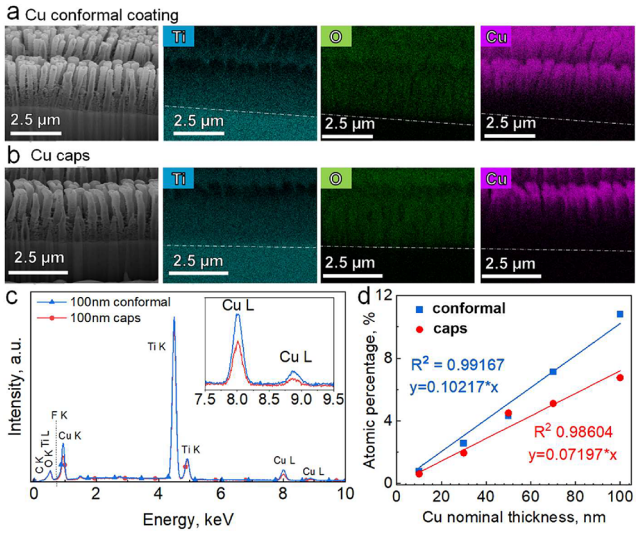

Figure 2. (a, b) FIB-SEM mapping of 100 nm Cu conformal (~10.5 atom % Cu) and cap (~7 atom % Cu coatings (FIB-SEM image and maps of Ti, O, and Cu, respectively) on 135 nm S nanotubes. (c) EDX spectra of nanotube layers with a nominal thickness of 100 nm Cu decoration (caps or conformal). (d) Atom % of Cu for different nominal thicknesses of Cu in a conformal (parallel) or cap (perpendicular) configuration.

In the conformal case, the Cu penetrated the tubes up to a depth of ~1.9 μm with a gradual decrease from top to bottom (Figure 2a). In contrast, in the cap morphology, the Cu was primarily confined to the uppermost ~0.35 μm of the tubes, which is consistent with depth-limited perpendicular sputtering (Figure 2b).

https://doi.org/10.1021/acsami.5c20633
ACS Appl. Mater. Interfaces 2026, 18, 6157–6165

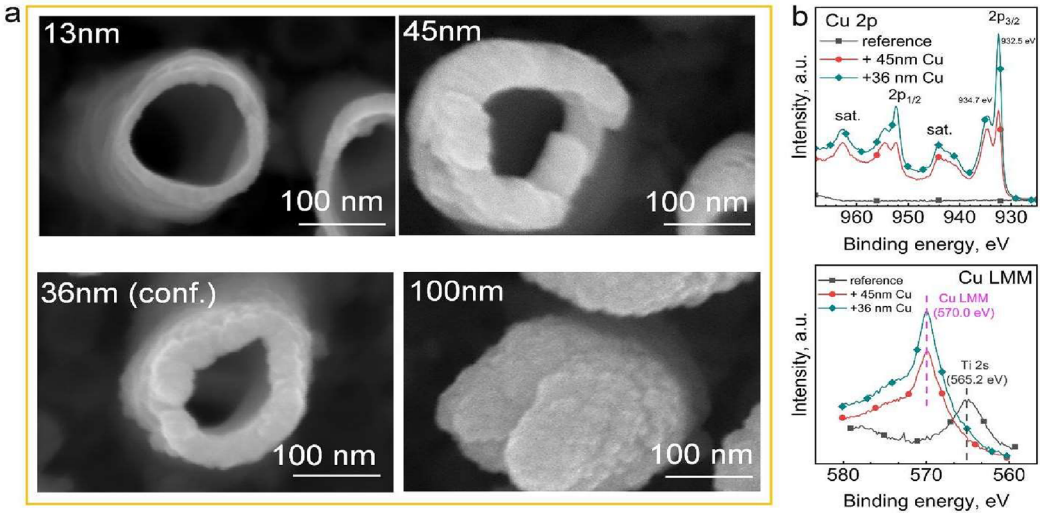

Figure 3. (a) High-resolution SEM images of the selected Cu decorations with the following nominal thicknesses: on spaced nanotubes with 135 nm spacing (caps configuration: 13, 45, and 100 nm, namely, ~1, ~3.3, and ~7 atom % Cu; and conformal coating 36 nm Cu with ~3.5 atom %). (b) High-resolution XPS spectra of bare NTs (reference) and of NTs with 45 nm Cu caps or 36 nm Cu conformal coating, showing the Cu 2p and the Cu LMM spectra.

This fabrication strategy yielded a reproducible platform of NTs with tunable intertube spacings. This enabled a systematic evaluation of how architecture influences Cu deposition geometry. Figure S8 shows SEM images of the different SP NTs with 100 nm nominal thickness of Cu sputtered in either conformal or capped conditions. The morphology with ~135 nm spacing was selected as the working configuration, because it offers optimal accessibility for directional Cu loading while maintaining spacing. Therefore, all subsequent Cu decoration and antibacterial assays were performed on this morphology, enabling controlled comparisons between cap and conformal geometries at different Cu loadings.

To correlate the nominal mass thickness of Cu sputtering with elemental incorporation, energy dispersive X-ray (EDX) analysis was performed (Figures 2c, S9, and S10). The Cu L peaks were confirmed at approximately 8.0 and 8.9 keV. Both the conformal and cap configurations exhibited a nearly linear increase in Cu content (atomic and weight percent) with nominal mass thickness (R^2 = 0.99 and 0.98, respectively; see Figures 2d and S10a). For equal nominal mass thickness, the cap configuration consistently contained less Cu than the conformal coating, e.g., 100 nm caps with ~7 atom % Cu and 100 nm conformal with ~10.5 atom % Cu. The distribution of Cu can also be observed in the high-resolution SEM images of the cross sections (Figure S11 shows this for a 70 nm Cu thickness).

Due to their large surface area, superior corrosion resistance, biocompatibility, and bioactivity, titanium dioxide nanotubes have drawn substantial attention as a potential platform for biomedical applications. However, to be applicable, the NTs must be carefully fabricated to ensure strong adhesion to the underlying metal substrate. Here, the mechanical properties of the bare NTs were studied quantitatively using the nano-indentation technique (Figure S12).[7] Hardness values (Figure S12a) measured at shallow indentation depths (~80 nm, i.e., <10% of the NT height, to minimize substrate influence)[32] were ~0.04 GPa. CP TiO_2 NTs exhibited the highest hardness among the different geometries, while the 210 nm SP NTs showed the lowest, indicating that increased intertube spacing reduces mechanical resistance, as expected. The corresponding elastic modulus values at a depth of 100 nm ranged from 1 to 2.5 GPa, with the CP NTs exhibiting the highest values (Figure S12b). These values are consistent with the porous, nanostructured nature of the layers and are far lower than bulk Ti (≈120−150 GPa).[7]

As a next step, both the CP and SP plain TiO_2 NT architectures were initially screened for their antibacterial performance. Although all SP morphologies exhibited similar levels of bacterial coverage, the 135 nm intertube spacing TiO_2 NTs, prepared with 5 wt % H_2O resulted in the least observed bacterial adherence (Figure S13). Thus, the 135 nm spaced TiO_2 NT morphology served as the standard platform to enable direct comparison across loading strategies for Cu deposition. In the cap configuration, sputtered thicknesses of 13, 45, and 100 nm of Cu corresponded to ~1, ~3.3, and ~7 atom % (atom % Cu), respectively. Additionally, a 36 nm conformal coating (~3.5 atom % Cu) was included for direct comparison of similar Cu content delivered via different geometries (conformal vs. caps). The corresponding top-view morphologies are shown in Figure 3a. These Cu levels are consistent with antibacterial activity thresholds reported in the literature (e.g., ~1 atom % for minimal cytotoxicity) and enable the dose-dependent evaluation of ion release and bacterial inhibition. Both the conformal and cap geometries ultimately degrade through Cu^{2+} ion release; however, their kinetics differ markedly, which can affect antibacterial functionality.

The presence and chemical state of Cu were further confirmed by X-ray photoelectron spectroscopy (XPS, Figures 3b and S14). The Cu 2p spectrum verifies the Cu incorporation in the decorated NTs, and the Ti 2p and O 1s spectra verify the TiO_2 matrix. Additional C 1s and O 1s contributions appeared after Cu decoration, with increased C−C, C−O, and C=O components, as well as suppressed Ti 2p/O−Ti signals (see the Supporting Information and Figure S14). Given the surface sensitivity of XPS, which is constrained to a maximum of 10 nm, and the sputtered nominal thickness of Cu, a Ti 2p signal was not observed in the XPS spectra, as it is covered by the sputtered Cu. More importantly, analysis of the Cu 2p and Cu LMM spectra (Figure 3b) revealed that the

https://doi.org/10.1021/acsami.5c20633
ACS Appl. Mater. Interfaces 2026, 18, 6157−6165

outer surface of the deposited Cu is predominantly of a $Cu(OH)_2$ thin layer (or a thin native CuO layer).[33−35] Specifically, the Cu $2p_{3/2}$ region shows a split, with peaks at 932.5 and 934.7 eV, corresponding to metallic Cu and $Cu(OH)_2$, respectively. There is also a characteristic satellite peak at ≈940−950 eV, which matches $Cu(OH)_2$ (for $Cu(OH)_2$, CuO, or Cu with native CuO. The peak-shape and the separation between the main peak to shakeup peak are quite different between the different chemical states.[34−36] The Cu LMM spectra further support this assignment by showing a peak position and shape consistent with $Cu(OH)_2$ or a native Cu oxide, rather than CuO or metallic Cu.[36] More importantly, the Cu chemistry is also confirmed from the O 1s peak (Figure S14b), where for the Cu decorated samples, no signal is detected for O from TiO_2 (see also Ti 2p in Figure S14c), but a shift in the O 1s peak to 531.5 eV is observed. This peak position is attributed to OH bonds to Cu, with a small shoulder at 530.5 eV corresponding to Cu−O bonds.[35]

The dissolution kinetics of Cu across loading strategies were then studied, and the results are summarized in Figure 4. As

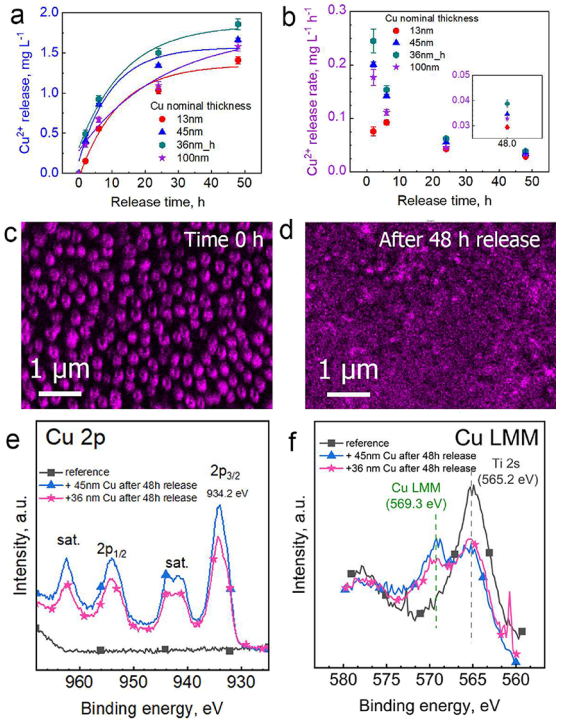

Figure 4. (a) Cu^{2+} release (mg L^{-1}) from ICP-AES for the tested Cu decorated samples (caps: 13 nm∼1 atom % Cu, 45 nm∼3.3, and 100 nm∼7 atom % Cu; and conformal coating 36 nm Cu (36 nm (conf.) with ∼3.5 atom %), and (b) corresponding Cu^{2+} release rate (mg L^{-1} h^{-1}); Cu maps from EDX for the 45 nm Cu-decorated spaced nanotubes, before (c) and after 48 h, (d) Cu release experiments. (e, f) high-resolution XPS spectra for the bare NTs (reference) and Cu-decorated NTs after 48 h release, namely, 45 nm Cu (caps) or 36 nm Cu (conformal coating), showing the Cu 2p and the Cu LMM spectra.

shown, the cap geometry minimized burst release. ICP-AES analysis showed lower Cu levels for the smaller cap (<2 mg L^{-1} after 48 h, see Figure 4a). The release rates followed the following order: conformal 36 > caps 45 > caps 100 > caps 13 nm (Figure 4b). This trend highlights the role of deposition geometry in controlling surface exposure and dissolution kinetics. The water contact angle (CA) and atomic force microscopy (AFM) imaging confirm that in the cap configuration, the reduced surface area exposed at the tube openings limited dissolution and promoted slower, sustained release (Figure S15a,c). This contrasts with the broader coverage of the conformal coating (Figure S15b,d). Evaluating Cu^{2+} release rates over time confirmed that thicker caps (45 or 100 nm) produced lower, yet sustained, release rates, which is consistent with their spatial confinement. In contrast, the lower release rate from the 13 nm caps reflects both reduced Cu mass and smaller exposed area.

A direct comparison with literature values is challenging due to variations in Cu^{2+} release conditions (e.g., sample area and solution volume).[14,23] For reference, our 135 nm SP TiO_2 NTs released approximately 1−1.5 mg L^{-1} Cu^{2+} after 24 h and 1.4−1.9 mg L^{-1} after 48 h (with a sample area ≈3 cm^2 immersed in 6 mL of water at 37 °C), whereas previous reports describe 0.06 mg L^{-1} at 7 days and 0.161 mg L^{-1} at 24 h. Importantly, the measured release values remain well below the reported safe threshold for Cu^{2+} in vivo (∼10 mg L^{-1}),[37,38] ensuring noncytotoxicity while maintaining antibacterial efficacy.

SEM-EDX mapping of the 45 nm caps before and after 48 h immersion (Figure 4c,d), revealed morphological changes consistent with progressive Cu^{2+} release. Some caps remained visible, and approximately 33% of the initial sputtered copper was still detected. Notably, there was no evidence of delamination or structural damage, as the nanotube morphology remained intact and clearly discernible in the EDX maps (see Figure S16).

XPS analysis after 48 h release confirmed the partial dissolution of the metallic Cu caps (Figure 4e,f). The 45 nm conformal and 36 nm caps coatings exhibited reduced Cu 2p intensity relative to the as-prepared samples. The reappearance of Ti 2p and O 1s signals from the underlying TiO_2 (Figure S17) clearly indicates the partial release of Cu. For both morphologies, (i) the Cu $2p_{3/2}$ at a lower binding energy of 934.2 eV indicated CuO (typically 933.8−964.0 eV),[33,34] and (ii) the shape of the Cu $2p_{3/2}$ satellite peak further corroborated CuO (Figure S18).[33,34] This assignment was consistent with the observed decrease and shift to lower binding energies in the Cu LMM peaks (569.3 eV)[35] and with the EDX findings.

The gradual reduction of Cu features is an intended outcome of the spatial decoration strategy and reflects controlled release rather than material failure. This sustained consumption under physiological exposure ensures long-term antibacterial efficacy while maintaining the nanotube architecture. These results indicate that nanotube geometry, through its influence on Cu localization, dictates the release kinetics: the cap configuration confines ion diffusion to the surface, whereas the conformal coating enables a slower, depth-dependent release. This geometry-controlled dissolution behavior explains the subsequent differences in antibacterial performance.

To assess the antibacterial effects of spaced TiO_2 NTs with different Cu loadings and configurations, we monitored bacterial growth of *Escherichia coli* (*E. coli*) by measuring the optical density at a wavelength of 600 nm ($OD_{600\ nm}$) (Figure 5a), starting from an initial $OD_{600\ nm}$ of 0.5 (∼5×10^7 CFU).[39] There was some effect on bacterial proliferation. A reduction in proliferation was evident, with the order of inhibition at 8 h being: 13 nm caps < 36 nm conformal/45 nm caps < 100 nm caps. These results suggest that higher Cu loading and a

https://doi.org/10.1021/acsami.5c20633
ACS Appl. Mater. Interfaces 2026, 18, 6157−6165

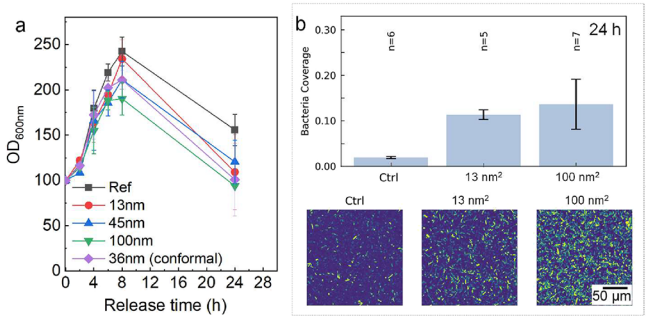

Figure 5. (**a**) Optical density ($OD_{600\ nm}$) measurements of the *E. coli* proliferation up to 24 h for bare, spaced NTs and Cu-decorated NTs with different morphologies and loadings (caps: 13 nm, ∼1 atom % Cu; 45 nm, ∼3.3 atom % Cu; 100 nm, ∼7 atom % Cu; and conformal coating 36 nm Cu (36 nm (conf.) with ∼3.5 atom %). (**b**) Representative fluorescence images of bacterial surface coverage at 24 h for selected samples: reference, 13 and 100 nm caps.

greater exposed surface area promote stronger initial antibacterial effects. Additionally, bacterial surface coverage at 24 h was evaluated for selected samples (reference SP NTs, 13 and 100 nm caps), see Figure 5b. Interestingly, the 100 nm cap-decorated NTs exhibited an increased bacterial presence after 24 h, suggesting that long-term adhesion may be influenced by a combination of Cu depletion and surface reorganization. While detailed mechanistic biological assays (e.g., cell viability or adhesion imaging) were beyond the scope of this materials development study, the present results establish a direct link between Cu morphology, release dynamics, and early bacterial inhibition. This reinforces the idea of a geometry-driven structure−function relationship.

Cu is well-known for its broad-spectrum antibacterial activity through multiple, synergistic mechanisms. Once released from the NT surface, Cu^{2+}/Cu^{+} ions interact with bacterial membranes, resulting in loss of permeability and leakage of intracellular components. Simultaneously, Cu participates in Fenton-like redox cycling, generating reactive oxygen species that damage lipids, proteins, and nucleic acids. Additionally, Cu ions can also bind to thiol-containing enzymes, disrupting essential metabolic pathways. The combined effects of Cu ions have been thoroughly researched and documented in the literature,[40,41] thus explaining the observed reduction in bacterial proliferation. $OD_{600\ nm}$ measurements show that discrepancies in Cu localization and, consequently, release kinetics between cap and conformal coatings result in varied antibacterial activity.

Overall, these results emphasize the importance of deposition geometry in determining Cu release and the antibacterial response. Leveraging the open architecture of spaced TiO_2 NTs, directional sputtering enables spatially selective Cu decoration, which dictates release kinetics and thus antibacterial performance. This geometry-driven approach offers a consistent option to adjust antibacterial function while maintaining nanotube integrity, creating a flexible foundation for designing multifunctional implant surfaces.

3. CONCLUSIONS

In this study, we present a spaced TiO_2 nanotube (NT) platform that is functionalized via geometry-controlled Cu decoration. This enables structure-tuned antibacterial activity. Through the combination of spaced, open-top NT architecture and directional sputtering, we achieved the selective deposition of either conformal wall coatings or discrete top caps. Cross-sectional SEM and AFM images, and EDX mapping confirmed this morphological control over Cu location, while ICP-AES demonstrated that cap morphologies minimize burst release and enable sustained Cu^{2+} delivery. With a loading of ∼1 atom % Cu (13 nm caps) measurable release produced moderate bacterial suppression at early time points. In contrast, higher loadings (e.g., 100 nm caps) contained more Cu overall; however, their cap geometry restricted dissolution, resulting in stronger inhibition at early time points. These findings highlight that the geometry of Cu distribution, in addition to total Cu content, plays a key role in shaping the antibacterial response. This approach prevents uncontrolled Cu aggregation while preserving the spaced nanotubular structure. It provides a scalable, reproducible method for antibacterial coatings with tunable release dynamics. Overall, this directional Cu decoration strategy establishes a design framework for multifunctional implant surfaces where spatially controlled metal deposition can be integrated with additional therapeutic functionalities.

4. EXPERIMENTAL SECTION

4.1. Anodization Procedures and Annealing

A 0.125 mm thick, 99.6% pure titanium foil (Advent, Oxford, UK) was used for the anodization process. The substrates were ultrasonically cleaned in acetone and ethanol for 5 min each. Then, the spaced nanotubes were prepared in an electrolyte containing diethylene glycol (DEG, > 99.5% p.a. Roth, Karlsruhe, Germany) + 2 wt % HF (HF 40%, Sigma-Aldrich, Germany) and X wt % H_2O, where X varied from 1 to 10 wt %. Anodization was performed in an O-ring cell with a diameter of 1 cm. A Pt mesh served as cathode, and a Ti foil served as the anode. The working distance between electrodes was 2 cm and 45 mL of electrolyte was used. As the anodization conditions were varied to achieve a specific morphology, they were adjusted as a function of the water content in the electrolyte, as follows: 1 wt % H_2O−47 V, 20 h; 5 wt % H_2O−40 V, 20 h; and 10 wt % H_2O−30 V, 20 h. The close-packed nanotubes were grown by anodization in a glycerol (>99.7% p.a. Roth, Karlsruhe, Germany):H_2O (70:30 vol %) solution containing 0.5 wt % NH_4F (>98% p.a. Roth, Karlsruhe, Germany), at 27 V for 3 h (similarly, a working distance of 1.5 cm and 45 mL of electrolyte were used). After anodization, the spaced NT samples were immersed in ethanol for 1 h to remove residual amounts of the anodization electrolyte. Then, samples were rinsed with distilled (DI) water and dried under a stream of N_2. The close-packed NTs were similarly washed with DI and dried. Both close-packed and spaced NTs were annealed at 400 °C for 1 h in air to convert the amorphous NTs into crystalline anatase fully.

4.2. Cu Decoration of the TiO_2 Nanotubes

Copper (Cu) was deposited onto the TiO_2 NT layers using a high-vacuum sputtering system (EM SCD500, Leica Mikrosysteme Vertrieb GmbH). Prior to deposition, Ar gas was introduced to reach an operating pressure of $\approx 10^{-2}$ mbar. The sputtering was conducted at a constant discharge current of 16 mA. Depending on the mounting orientation of the sample relative to the target, two deposition geometries were obtained: (i) when the samples are aligned parallel to the target (0° angle), a conformal Cu coating formed along the NT walls, and (ii) when the samples are positioned perpendicular to the target (90° angle), Cu accumulated preferentially at the tube openings, producing discrete cap-like features. The deposited Cu thickness was controlled by an integrated quartz crystal film-thickness monitor. It should be noted that after Cu sputtering, no postdeposition annealing treatments were carried out.

https://doi.org/10.1021/acsami.5c20633
ACS Appl. Mater. Interfaces 2026, 18, 6157−6165

4.3. Morphology, Physical and Chemical Characterizations

The morphology of the nanotubular layers, including tube diameter, spacing, and tube length, was evaluated using a scanning electron microscope (SEM, FE-SEM 4800SEM, Hitachi, Japan) from three different spots on each sample. Moreover, for the statistical analysis of tube diameter and intratube spacing, the values were averaged across 3 distinct samples for each morphology, with 3 independent images (×100k magnification) for each sample. For the Cu-decorated samples, energy dispersive X-ray spectroscopy (EDX) coupled with the SEM was used to evaluate the layer's chemical composition.

The chemical composition was characterized using X-ray photoelectron spectroscopy (XPS, PHI 5600, US), and we calibrated the spectra with the C 1s peak at 284.8 eV. For samples, where a Ti 2p signal was also visible, we checked the calibration with the Ti 2p peak at 459.0 eV.

Surface and cross-sectional observations of Cu-decorated NTs were performed using ZEISS FIB-SEM Crossbeam 550 system with high-resolution. Focused ion beam (FIB) milling with a gallium ion source was used to prepare cross sections of the samples. This procedure was carried out in three sequential steps with an accelerating voltage of 30 kV and gradually decreasing beam currents of 700, 300, and 100 pA. This minimizes the curtaining effect and achieves fine polishing of the NTs' surface and internal structure. The total dwell time for the FIB cut was 12 min. To determine the presence and localization of Cu, an energy-dispersive X-ray spectroscopy (EDX) analysis was performed using an Oxford Instruments Ultim Max 170 Silicon Drift Detector, integrated into the FIB-SEM system. Elemental mappings were acquired on the top surface and the cross-sectional areas of the samples to assess the spatial distribution of copper relative to the TiO_2 matrix. Measurements were conducted at an accelerating voltage of 16 kV, sufficient for detecting and mapping the Cu Kα line. Data acquisition and analysis were carried out using AZtecEnergy software.

Apparent water contact angle measurements were performed using a KRUSS DSA25 drop shape analyzer. In the standard experiment, 5 μL of DI water was dispersed on the sample surface using a liquid needle approach. The water droplet was allowed to rest on the surface until it reached a constant shape. Consequently, the apparent water contact angle was obtained using the Laplace−Young model fitting with KRUSS ADVANCE software.

The morphology of the NT samples was obtained using a Park NX20 atomic force microscope (AFM, Park Systems, Suwon, Korea). Measurements were performed in noncontact mode with an AC-160TS cantilever featuring a high resonant frequency of 300 kHz, a force constant of 26 N m^{-1}, and a tip radius of about 7 nm. All images were acquired at a resolution of 1024 × 1024 pixels, with a scan rate in the range between 0.05 and 0.5 Hz, and a scan range of 4 μm^2. The AFM images were analyzed using Gwyddion 2.68 software.

Nanoindentation measurements were performed in continuous stiffness measurement (CSM) mode using a Nanoindenter XP (Keysight, Colorado Springs, CO, USA) with a diamond Berkovich tip (Synton-MDP, Nidau, Switzerland). Indentation depths of up to 900 nm were reached, based on the length of the NTs (as also previously reported[7]). The samples were mounted on an aluminum holder using Crystal Bond thermal adhesive after being cleaned with isopropyl alcohol. The adhesive was melted by heating the holder to 150 °C and then positioning the sample. Measurements were conducted at ambient conditions after 3 h of thermal stabilization, achieving a drift rate of ≤0.05 nm s^{-1}. To determine hardness and elastic modulus, 10 indents were performed for each NT morphology (adjacent indents were spaced 10 μm apart).

4.4. Cu^{2+}-Ion Release Experiments

Inductively coupled plasma atomic emission spectroscopy (ICP-AES) (Ciros CCD, Spectro Analytical Instruments GmbH, Germany) was used to investigate the release of Cu^{2+} ions from various Cu-decorated TiO_2 NT layers, upon immersion in deionized water at 37 °C. Copper ion concentrations were determined by monitoring the emission line at 324.754 nm, with argon (Ar) serving as the internal standard at 430.010 nm. All measurements were performed in duplicate, and the reported values represent the average Cu^{2+} concentrations, expressed in mg L^{-1}. Three identical samples of each of the investigated Cu-decorated samples (each with an NT area diameter of 1.1 cm and a surface area of 0.97 cm^2) were immersed in 6 mL of ultrapure water, and the cumulative ion release was assessed at 2, 6, 24, and 48 h at 37 °C.

4.5. Antibacterial Experiments

The antibacterial efficacy of Cu-decorated, space-packed TiO_2 NTs, as well as bare NT coatings, was evaluated against Gram-negative *Escherichia coli* (*E. coli*) bacteria. Isolated bacterial colonies were suspended in 5 mL of LB medium (Carl Roth, Karlsruhe, Germany) and incubated overnight at 37 °C with agitation at 150 rpm using an orbital shaker under approximately 80% humidity. The resulting bacterial suspension was then diluted to an optical density (OD) of approximately 0.5, as measured at 600 nm wavelength using a Biophotometer Plus (Eppendorf AG, Hamburg, Germany), as also detailed in previous works.[42,43]

Each sample was placed in an individual well of a multiwell plate containing 5 mL of the diluted bacterial suspension, after which the plate was incubated at 37 °C. Initial screening was performed using close-packed and differently spaced NT layers. For the Cu-functionalized nanotubes, bare spaced NT coatings (prepared using DEG + 2 wt % HF + 5 wt % H_2O) served as reference, while the corresponding Cu-decorated samples represented the test group. Optical density ($OD_{600\ nm}$) measurements were taken at 2, 4, 6, 8, 24, and 48 h by withdrawing an aliquot from each well, measuring the $OD_{600\ nm}$, and then returning the aliquot to its respective well to maintain a consistent volume and set of conditions. To ensure statistical relevance, three replicates were performed for each sample type.

For selected experiments, fluorescently labeled *E. coli* strains were used. To assess bacterial adhesion directly, the specimens were removed after incubation. They were then gently rinsed with phosphate-buffered saline (PBS) to eliminate any bacteria that were loosely attached using an upright laser scanning confocal microscope system (Leica, SP5) with a 20×/1.0 NA dip-in objective lens.

■ ASSOCIATED CONTENT

Supporting Information

The Supporting Information is available free of charge at https://pubs.acs.org/doi/10.1021/acsami.5c20633.

Figure S1: Cross-sectional images of CP and SP nanotube layers with different spacings; Figure S2: histograms for nanotube diameter and spacing for the 135 nm spaced TiO_2 nanotube; Figure S3: water contact angles as measured on the CP and SP TiO_2 nanotube layers with different spacings; Figure S4: SEM images of the 135 nm spacing SP TiO_2 nanotube with conformal or cap Cu coating with 100 nm nominal thickness; Figure S5: SEM images of the CP TiO_2 nanotube with conformal or cap Cu coating with 100 nm nominal thickness; Figure S6: SEM images and corresponding EDX mapping of the 100 nm Cu conformal decoration of 135 nm spaced TiO_2 NTs; Figure S7: SEM images and corresponding EDX mapping of the 100 nm Cu cap decoration of 135 nm spaced TiO_2 NTs; Figure S8: spaced NTs with different spacings (70, 135, or 210 nm) for 100 nm nominal thickness Cu decoration in conformal or caps configuration; Figure S9: EDX spectra for selected (10, 50, or 100 nm) Cu nominal thickness in conformal or cap configuration on 135 nm spacing of spaced NTs; Figure S10: EDX data (weight percentage, atomic percentage) and trendline for weight percentage for the conformal or cap configuration on 135 nm spacing SP TiO_2 nanotubes; Figure S11: high-resolution SEM images of the cross-section of the 70 nm nominal

https://doi.org/10.1021/acsami.5c20633
ACS Appl. Mater. Interfaces 2026, 18, 6157−6165

thickness Cu decoration in conformal or cap configuration on 135 nm spacing TiO_2 nanotubes; Figure S12: nanoindentation measurements for bare TiO_2 nanotube (CP and SP nanotube layers); Figure S13: bacterial coverage of different bare TiO_2 nanotube morphologies; Figure S14: high-resolution XPS spectra (C 1s, O 1s, and Ti 2p) for 135 nm spacing NTs (reference, 36 nm conformal or 45 nm caps Cu decoration); Figure S15: water contact angles and 3D reconstruction AFM images of 135 nm SP NTs with 36 nm conformal or 45 nm caps Cu decoration; Figure S16: SEM-EDX maps of 135 nm SP NTs with 36 nm conformal or 45 nm caps Cu decoration after 48 h release experiments; Figure S17: high-resolution XPS spectra (C 1s, O 1s, and Ti 2p) for 135 nm spacing NTs (reference) and after 48 h release for 36 nm conformal or 45 nm caps Cu decoration; Figure S18: overlay of the Cu $2p_{3/2}$ satellite peak (XPS) for both 45 nm Cu caps and 36 nm Cu conformal decoration, before and after 48 h release experiments (PDF)

AUTHOR INFORMATION

Corresponding Authors

Alexander B. Tesler − *Department of Physics, Biophysics Group, Friedrich-Alexander-Universität Erlangen-Nürnberg, Erlangen 91052, Germany; Department of Materials Engineering, Faculty of Engineering, Bar Ilan University, Ramat-Gan 5290002, Israel;* orcid.org/0000-0003-3425-7667; Email: alexander.tesler@biu.ac.il

Anca Mazare − *Department of Materials Science and Engineering, Institute for Surface Science and Corrosion, Faculty of Engineering, Friedrich-Alexander-Universität Erlangen-Nürnberg, Erlangen 91058, Germany;* orcid.org/0000-0002-4836-946X; Email: anca.mazare@fau.de

Authors

Markus Pach − *Department of Materials Science and Engineering, Institute for Surface Science and Corrosion, Faculty of Engineering, Friedrich-Alexander-Universität Erlangen-Nürnberg, Erlangen 91058, Germany*

David Böhringer − *Department of Physics, Biophysics Group, Friedrich-Alexander-Universität Erlangen-Nürnberg, Erlangen 91052, Germany*

Iana Fomicheva − *Department of Physics, Biophysics Group, Friedrich-Alexander-Universität Erlangen-Nürnberg, Erlangen 91052, Germany; Fraunhofer Institute for Ceramic Technologies and Systems IKTS, Forchheim 91301, Germany; Department of Physics, Friedrich-Alexander-Universität Erlangen-Nürnberg, Erlangen 91058, Germany*

George Sarau − *Fraunhofer Institute for Ceramic Technologies and Systems IKTS, Forchheim 91301, Germany; Institute for Nanotechnology and Correlative Microscopy gGmbH (INAM), Forchheim 91301, Germany; Max Planck Institute for the Science of Light, Erlangen 91058, Germany*

Nicola Taccardi − *Lehrstuhl für Chemische Reaktionstechnik (CRT), Friedrich-Alexander-Universität Erlangen-Nürnberg, Erlangen 91058, Germany*

Maksim Kamaleev − *Department of Materials Science and Engineering, Chair of General Materials Properties, Friedrich-Alexander-University of Erlangen-Nürnberg, Erlangen 91058, Germany;* orcid.org/0000-0003-3826-2893

Silke H. Christiansen − *Fraunhofer Institute for Ceramic Technologies and Systems IKTS, Forchheim 91301, Germany; Institute for Nanotechnology and Correlative Microscopy gGmbH (INAM), Forchheim 91301, Germany; Physics Department, Freie Universität Berlin, Berlin 14195, Germany;* orcid.org/0000-0002-4908-4087

Wolfgang H. Goldmann − *Department of Physics, Biophysics Group, Friedrich-Alexander-Universität Erlangen-Nürnberg, Erlangen 91052, Germany;* orcid.org/0000-0003-0738-2665

Complete contact information is available at: https://pubs.acs.org/10.1021/acsami.5c20633

Notes

The authors declare no competing financial interest.

ACKNOWLEDGMENTS

I.F., A.B.T., and W.H.G. thank the Deutsche Forschungsgemeinschaft (DFG) for financial support (award number 540989797). I.F., G.S., and S.C. were supported by the European Union's H2020 research and innovation program through the Marie Sklodowska-Curie grant agreement AIMed ID: 861138, and the research projects 4D+ nanoSCOPE ID: 810316 and LRI ID: C10, STOP ID: 101057961; the German Research Foundation (DFG) within the research project UNPLOK ID: 523847126, and from the "Freistaat Bayern" and the European Union within the project Analytiktechnikum für Gesundheits- und Umweltforschung AGEUM, project (StMWi-43-6623-22/1/3).

REFERENCES

(1) Roy, P.; Berger, S.; Schmuki, P. TiO_2 Nanotubes: Synthesis and Applications. *Angew. Chem., Int. Ed.* **2011**, *50* (13), 2904−2939.

(2) Macak, J. M.; Tsuchiya, H.; Taveira, L.; Ghicov, A.; Schmuki, P. Self-Organized Nanotubular Oxide Layers on Ti-6Al-7Nb and Ti-6Al-4V Formed by Anodization in NH_4F Solutions. *J. Biomed Mater. Res. A* **2005**, *75* (4), 928−933.

(3) Park, J.; Tesler, A. B.; Gongadze, E.; Iglič, A.; Schmuki, P.; Mazare, A. Nanoscale Topography of Anodic TiO_2 Nanostructures Is Crucial for Cell−Surface Interactions. *ACS Appl. Mater. Interfaces* **2024**, *16* (4), 4430−4438.

(4) Park, J.; Bauer, S.; Von Der Mark, K.; Schmuki, P. Nanosize and Vitality: TiO_2 Nanotube Diameter Directs Cell Fate. *Nano Lett.* **2007**, *7* (6), 1686−1691.

(5) Brammer, K. S.; Oh, S.; Cobb, C. J.; Bjursten, L. M.; van der Heyde, H.; Jin, S. Improved Bone-Forming Functionality on Diameter-Controlled TiO_2 Nanotube Surface. *Acta Biomater.* **2009**, *5* (8), 3215−3223.

(6) Necula, M. G.; Mazare, A.; Ion, R. N.; Ozkan, S.; Park, J.; Schmuki, P.; Cimpean, A. Lateral Spacing of TiO_2 Nanotubes Modulates Osteoblast Behavior. *Materials* **2019**, *12* (18), 2956.

(7) Negrescu, A. M.; Ionascu, I.; Necula, M. G.; Tudor, N.; Kamaleev, M.; Zarnescu, O.; Mazare, A.; Schmuki, P.; Cimpean, A. Lateral Spacing of TiO_2 Nanotube Coatings Modulates In Vivo Early New Bone Formation. *Biomimetics* **2025**, *10* (2), 81.

(8) Nguyen, N. T.; Ozkan, S.; Hwang, I.; Mazare, A.; Schmuki, P. TiO2 Nanotubes with Laterally Spaced Ordering Enable Optimized Hierarchical Structures with Significantly Enhanced Photocatalytic H_2 Generation. *Nanoscale* **2016**, *8* (38), 16868−16873.

(9) Ozkan, S.; Nguyen, N. T.; Hwang, I.; Mazare, A.; Schmuki, P. Highly Conducting Spaced TiO_2 Nanotubes Enable Defined Conformal Coating with Nanocrystalline Nb_2O_5 and High Performance Supercapacitor Applications. *Small.* **2017**.

(10) Linklater, D. P.; Baulin, V. A.; Juodkazis, S.; Crawford, R. J.; Stoodley, P.; Ivanova, E. P. Mechano-Bactericidal Actions of Nanostructured Surfaces. *Nat. Rev. Microbiol* **2021**, *19* (1), 8−22.
(11) Senevirathne, S. W. M. A. I.; Hasan, J.; Mathew, A.; Woodruff, M.; Yarlagadda, P. K. D. V. Bactericidal Efficiency of Micro- and Nanostructured Surfaces: A Critical Perspective. *RSC Adv.* **2021**, *11* (3), 1883−1900.
(12) Zhao, L.; Wang, H.; Huo, K.; Cui, L.; Zhang, W.; Ni, H.; Zhang, Y.; Wu, Z.; Chu, P. K. Antibacterial Nano-Structured Titania Coating Incorporated with Silver Nanoparticles. *Biomaterials* **2011**, *32* (24), 5706−5716.
(13) Durán, N.; Durán, M.; de Jesus, M. B.; Seabra, A. B.; Fávaro, W. J.; Nakazato, G. Silver Nanoparticles: A New View on Mechanistic Aspects on Antimicrobial Activity. *Nanomedicine* **2016**, *12* (3), 789−799.
(14) Fabian, J.; Morton, G.; Sharma, S.; Duffy, B.; Warren, S. Effect of Electrodeposition Time on Physical Characteristics and Antibacterial Activity of Copper-Incorporated TiO_2 Nanotubes. *RSC Adv.* **2025**, *15* (1), 142−156.
(15) Rosenbaum, J.; Versace, D. L.; Abbad-Andallousi, S.; Pires, R.; Azevedo, C.; Cénédese, P.; Dubot, P. Antibacterial Properties of Nanostructured Cu−TiO_2 Surfaces for Dental Implants. *Biomater Sci.* **2017**, *5* (3), 455−462.
(16) Liu, N.; Jha, H.; Hahn, R.; Schmuki, P. Palladium Activated Decoration of TiO_2 Nanotubes by Copper Nanoparticles and Enhanced Photocatalytic Properties. *ECS Electrochemistry Letters* **2012**, *1* (6), H29−H31.
(17) Macak, J. M.; Gong, B. G.; Hueppe, M.; Schmuki, P. Filling of TiO_2 Nanotubes by Self-Doping and Electrodeposition. *Adv. Mater.* **2007**, *19* (19), 3027−3031.
(18) Zhang, S.; Zhang, S.; Peng, F.; Zhang, H.; Liu, H.; Zhao, H. Electrodeposition of Polyhedral Cu_2O on TiO_2 Nanotube Arrays for Enhancing Visible Light Photocatalytic Performance. *Electrochem. Commun.* **2011**, *13* (8), 861−864.
(19) Savargaonkar, A. V.; Munshi, A. H.; Soares, P.; Popat, K. C. Antifouling Behavior of Copper-Modified Titania Nanotube Surfaces. *J. Funct Biomater* **2023**, *14* (8), 413.
(20) Hang, R.; Gao, A.; Huang, X.; Wang, X.; Zhang, X.; Qin, L.; Tang, B. Antibacterial Activity and Cytocompatibility of Cu−Ti−O Nanotubes. *J. Biomed Mater. Res. A* **2014**, *102* (6), 1850−1858.
(21) Mahmoudi-Qashqay, S.; Zamani-Meymian, M.-R.; Sadati, S. J. Improving Antibacterial Ability of Ti-Cu Thin Films with Co-Sputtering Method. *Sci. Rep* **2023**, *13* (1), 16593.
(22) Koklic, T.; Urbančič, I.; Zdovc, I.; Golob, M.; Umek, P.; Arsov, Z.; Dražić, G.; Pintarič, Š.; Dobeic, M.; Štrancar, J. Surface Deposited One-Dimensional Copper-Doped TiO_2 Nanomaterials for Prevention of Health Care Acquired Infections. *PLoS One* **2018**, *13* (7), No. e0201490.
(23) Chen, H.; Zhang, J.; Yang, F.; Lin, T.; Zhang, J.; Cai, X.; Zhang, P.; Tan, S. Implanting a Copper Ion into a TiO 2 Nanorod Array for the Investigation on the Synergistic Antibacterial Mechanism between Mechanical Cracking and Chemical Damage. *ACS Biomater Sci. Eng.* **2022**, *8* (4), 1464−1475.
(24) Shimabukuro, M.; Tsutsumi, Y.; Nozaki, K.; Chen, P.; Yamada, R.; Ashida, M.; Doi, H.; Nagai, A.; Hanawa, T. Investigation of Antibacterial Effect of Copper Introduced Titanium Surface by Electrochemical Treatment against Facultative Anaerobic Bacteria. *Dent Mater. J.* **2020**, *39* (4), 639−647.
(25) Zhang, X.; Li, J.; Wang, X.; Wang, Y.; Hang, R.; Huang, X.; Tang, B.; Chu, P. K. Effects of Copper Nanoparticles in Porous TiO_2 Coatings on Bacterial Resistance and Cytocompatibility of Osteoblasts and Endothelial Cells. *Materials Science and Engineering: C* **2018**, *82*, 110−120.
(26) Aoki, S.; Shimabukuro, M.; Kishida, R.; Kyuno, K.; Noda, K.; Yokoi, T.; Kawashita, M. Electrochemical Deposition of Copper on Bioactive Porous Titanium Dioxide Layer: Antibacterial and Pro-Osteogenic Activities. *ACS Appl. Bio Mater.* **2023**, *6* (12), 5759−5767.
(27) Kang, S. H.; Sung, Y.-E.; Smyrl, W. H. The Effectiveness of Sputtered PtCo Catalysts on TiO_2 Nanotube Arrays for the Oxygen Reduction Reaction. *J. Electrochem. Soc.* **2008**, *155* (11), B1128.
(28) Nguyen, N. T.; Altomare, M.; Yoo, J. E.; Taccardi, N.; Schmuki, P. Noble Metals on Anodic TiO_2 Nanotube Mouths: Thermal Dewetting of Minimal Pt Co-Catalyst Loading Leads to Significantly Enhanced Photocatalytic H_2 Generation. *Adv. Energy Mater.* **2016**, *6* (2), No. 1501926.
(29) Yoo, J. E.; Lee, K.; Schmuki, P. Dewetted Au Films Form a Highly Active Photocatalytic System on TiO_2 Nanotube-Stumps. *Electrochem. Commun.* **2013**, *34*, 351−355.
(30) Afshar, M.; Ghosh, S.; Mascaretti, L.; Kment, Š.; Casari, C. S.; Naldoni, A. Spaced Hybrid TiO_2 /Au Nanotube Arrays with Tailored Optical Properties for Surface-Enhanced Raman Scattering. *ACS Omega* **2024**, *9* (49), 48205−48212.
(31) Ozkan, S.; Mazare, A.; Schmuki, P. Critical Parameters and Factors in the Formation of Spaced TiO_2 Nanotubes by Self-Organizing Anodization. *Electrochim. Acta* **2018**, *268*, 435.
(32) Xu, Y. N.; Liu, M. N.; Wang, M. C.; Oloyede, A.; Bell, J. M.; Yan, C. Nanoindentation Study of the Mechanical Behavior of TiO_2 Nanotube Arrays. *J. Appl. Phys.* **2015**, *118* (14), 145301.
(33) Biesinger, M. C. Advanced Analysis of Copper X-ray Photoelectron Spectra. *Surf. Interface Anal.* **2017**, *49* (13), 1325−1334.
(34) Biesinger, M. C.; Lau, L. W. M.; Gerson, A. R.; Smart, R. S. C. Resolving Surface Chemical States in XPS Analysis of First Row Transition Metals, Oxides and Hydroxides: Sc, Ti, V, Cu and Zn. *Appl. Surf. Sci.* **2010**, *257* (3), 887−898.
(35) Platzman, I.; Brener, R.; Haick, H.; Tannenbaum, R. Oxidation of Polycrystalline Copper Thin Films at Ambient Conditions. *J. Phys. Chem. C* **2008**, *112* (4), 1101−1108.
(36) Miura, R.; Kitada, A.; Fukami, K.; Murase, K. Thermodynamic Design of Electrolyte for CuO/Cu_2O Bilayer by Anodic Electrodeposition. *J. Electrochem. Soc.* **2021**, *168* (6), No. 062506.
(37) Xia, C.; Ma, X.; Zhang, X.; Li, K.; Tan, J.; Qiao, Y.; Liu, X. Enhanced Physicochemical and Biological Properties of C/Cu Dual Ions Implanted Medical Titanium. *Bioact Mater.* **2020**, *5* (2), 377−386.
(38) Burghardt, I.; Lüthen, F.; Prinz, C.; Kreikemeyer, B.; Zietz, C.; Neumann, H.-G.; Rychly, J. A Dual Function of Copper in Designing Regenerative Implants. *Biomaterials* **2015**, *44*, 36−44.
(39) Tesler, A. B.; Prado, L. H.; Khusniyarov, M. M.; Thievessen, I.; Mazare, A.; Fischer, L.; Virtanen, S.; Goldmann, W. H.; Schmuki, P. A One-Pot Universal Approach to Fabricate Lubricant-Infused Slippery Surfaces on Solid Substrates. *Advanced Functional Materials.* **2021**.
(40) Salah, I.; Parkin, I. P.; Allan, E. Copper as an Antimicrobial Agent: Recent Advances. *RSC Adv.* **2021**, *11* (30), 18179−18186.
(41) Grass, G.; Rensing, C.; Solioz, M. Metallic Copper as an Antimicrobial Surface. *Appl. Environ. Microbiol.* **2011**, *77* (5), 1541−1547.
(42) Gritsch, L.; Lovell, C.; Goldmann, W. H.; Boccaccini, A. R. Fabrication and Characterization of Copper(II)-Chitosan Complexes as Antibiotic-Free Antibacterial Biomaterial. *Carbohydr. Polym.* **2018**, *179*, 370−378.
(43) Yang, Y.; Zheng, K.; Liang, R.; Mainka, A.; Taccardi, N.; Roether, J. A.; Detsch, R.; Goldmann, W. H.; Virtanen, S.; Boccaccini, A. R. Cu-Releasing Bioactive Glass/Polycaprolactone Coating on Mg with Antibacterial and Anticorrosive Properties for Bone Tissue Engineering. *Biomedical Materials* **2018**, *13* (1), No. 015001.

https://doi.org/10.1021/acsami.5c20633
ACS Appl. Mater. Interfaces 2026, 18, 6157−6165